Chemical durability of uranium oxide microspheres for use as QC materials for nuclear safeguards

Nicolas Clavier, Pierre Asplanato, Wassima Zannouh, Anne-Laure Fauré, Manon Cornaton, Nicolas Dacheux, Fabien Pointurier

Chemical durability of uranium oxide microspheres for use as QC materials for nuclear safeguards

Nicolas Clavier [1,], Pierre Asplanato [1,2], Wassima Zannouh [1], Anne-Laure Fauré [2], Manon Cornaton [2], Nicolas Dacheux [1], Fabien Pointurier [2]*

[1] ICSM, Univ Montpellier, CEA, CNRS, ENSCM, Marcoule, France

[2] CEA, DAM, DIF, 91297 Arpajon, France

Full contact information :

1- ICSM, Univ Montpellier, CEA, CNRS, ENSCM
Site de Marcoule
BP 17171
30207 Bagnols sur Cèze
France

2- CEA/DAM Ile de France
91297 Arpajon Cedex
France

**** Corresponding author :***

Nicolas CLAVIER
Email : nicolas.clavier@icsm.fr
Phone : + 33 4 66 33 92 08

Abstract :

This study investigates the chemical durability of uranium oxide microparticles (UO_{2+x} and U_3O_8), as potential reference materials for nuclear safeguards. To optimize long-term preservation, the particles were exposed to three different storage media: dilute nitric acid (10^{-2} $mol.L^{-1}$ HNO_3), deionised water, and ethanol. Dissolution rates in nitric acid (~5×10^{-4} $g.m^{-2}.d^{-1}$) were similar to those of bulk uranium oxides, but UO_{2+x} particles experienced greater absolute leaching due to their higher specific surface area, resulting in noticeable morphological changes. In distilled water, rapid precipitation of secondary phases, such as schoepite and studtite, transformed particle morphology into aggregated platelets. In contrast, ethanol preserved both particle shape and structural integrity over eight months, ensuring stability for isotopic analysis using Large Geometry Secondary Ion Mass Spectrometry (LG-SIMS). These results suggest ethanol as the most effective storage medium, especially under anhydrous conditions. While both UO_{2+x} and U_3O_8 exhibited comparable durability, their reactivity was primarily influenced by microstructural differences. This study highlights the importance of selecting appropriate storage conditions based on fabrication methods and particle characteristics to maintain uranium oxide reference materials for nuclear safeguards and ensure their long-term reliability in quality control applications.

Keywords :

Nuclear safeguards; Uranium oxides; Microparticles; Chemical durability; Isotopic measurements

1. Introduction

The International Atomic Energy Agency (IAEA) inspects facilities of its member states to assess their compliance with nuclear material safeguards obligations in the frame of the non-proliferation treaty. IAEA inspectors routinely collect particulate matter at nuclear facilities by wiping smooth surfaces at various locations inside the facility using square pieces of cotton cloths, called “environmental” or “swipe samples”. This particulate matter contains nanometer to micrometer sized fragments, so-called particles, of nuclear material that has been processed. Because the isotopic and elemental compositions of these particles are representative of the original material, these particles can be considered as fingerprints of specific processes of the nuclear industry [1, 2]. The swipe samples are analyzed by a small number of specialized laboratories. The main aim of the analyses carried out by these laboratories is to detect and characterize individual particles of nuclear material (U and/or Pu), primarily to determine their isotopic composition. These analyses make it possible to verify the declarations made by the operators of nuclear facilities and to detect any undeclared activities. Secondary ion mass spectrometry [3, 4] and fission track thermal ionization mass spectrometry [5, 6] are the relevant techniques for determining the isotopic composition of such particles. The main difficulty arises from the small number of particles collected during sampling and their small size, generally close to or even less than one micrometer. Under these conditions, it is essential to have reference particles whose size, density and chemical

and isotopic compositions are perfectly known in order to develop and optimize the analytical methodologies implemented in the laboratories, and to ensure the quality control (QC) of the particle analysis.

With this goal in mind, several groups have developed, in recent years, original synthesis routes for the preparation of microspheres of actinide oxides (An = Th, U, Pu) and lanthanides. These are prepared by a variety of methods, such as aerosol pyrolysis [7, 8] or hydrothermal conversion of actinide carboxylates [9-11]. In both cases, spherical particles with diameters typically between 200 nm and a few µm are obtained, with UO_{2+x} or U_3O_8 formulations (eventually doped with thorium or plutonium), depending on the synthesis route envisaged. Once prepared, these particles can be stored as powders or suspensions, the latter having the advantage of being more convenient for the preparation of test samples by simple spraying on a chosen support (pad, textile, plant sample, etc.). This method of preservation, which can last from several weeks to several years, raises the question of the chemical stability of the particles in the chosen solvent.

To date, there is little data on the chemical durability of uranium oxide microparticles. Recent studies [12-14] have shown that particles with U_3O_8 formulation prepared by aerosol pyrolysis were not significantly altered after several months in contact with an alcoholic solution (unchanged morphology, negligible mass loss). Conversely, the formation of secondary phases has been reported in aqueous media, leading to a drastic change in particle morphology [14]. In each of these cases, however, no kinetic data are reported, making it difficult to estimate the lifetime of the particle in these solvents. On the other hand, the kinetics of uranium oxide leaching/dissolution in aqueous media are well documented, particularly in view of the high stakes involved in the reprocessing or deep geological disposal of spent nuclear fuel [15-20]. The results reported in the literature are mostly in the form of normalized dissolution rates (expressed in $g.m^{-2}.day^{-1}$), possibly supplemented by kinetic and thermodynamic data allowing an empirical description of the impact of operating conditions on the dissolution reaction (activation energy, partial orders, etc.).

At the crossroads of these two approaches, this article investigates the chemical durability of hydrothermally prepared uranium oxide microspheres (UO_{2+x} or U_3O_8) in different media. First, the study of particles alteration in nitric media allowed us to easily measure dissolution rates and compare the properties of micrometric particles with those of bulk materials. Secondly, the behavior of the particles in deionised water was studied in order to highlight the conditions for the formation of potential neoformed phases in solution or at the solid/solution interface, which could occur during the conservation of reference materials in humid atmosphere. Finally, chemical durability tests in ethanol were undertaken to validate the potential use of this medium for particle conservation. Irrespective of the medium used, the particles were characterized after contact with the solution, either structurally (X-Ray Diffraction - XRD, Raman spectrometry), morphologically (Scanning Electron Microscopy - SEM) or isotopically (Large Geometry Secondary Ion Mass Spectrometry - LG-SIMS). The results reported in this manuscript thus enable us to propose recommendations for the preservation of uranium oxide particles with a view to their use in international nuclear safeguards.

2. Materials and methods

Caution! ^{238}U, the major isotope of natural uranium, is an α emitter radionuclide and is considered as a health hazard. Experiments involving natural uranium require appropriate facilities and personnel trained in the handling of radioactive materials.

2.1. Microparticles synthesis

All the conventional chemicals were supplied by Sigma and were of analytical grade, while uranium was kindly provided by CETAMA (Commission d'Etablissement des Méthodes d'Analyse, CEA Marcoule, France). This latter was converted from uranium metal chips to U(IV) in hydrochloric acid solution by dissolution in 6 mol.L^{-1} HCl, as described in [21]. The preparation of UO_{2+x} and U_3O_8 particles was undertaken following the protocol originally reported by Trillaud *et al.* [9] and based on the initial mixture of aspartic acid (1.5 mmol) and U(IV) in hydrochloric media (0.5 mmol). The pH of the solution was maintained at about 2 by adding 4 mol.L^{-1} ammonia solution, which rapidly led to the formation of a greenish precipitate. Both the solid phase and the supernatant were then transferred to a Teflon-lined autoclave (Parr) and hydrothermally treated at 160°C for 30 hours. During this heat treatment, the reacting media were constantly stirred using a magnetic stirrer (2Mag – MixControl 20). The stirring speed, and thus the Reynolds number (Re_A), was adjusted as described in [9] to monitor the hydrodynamics inside the reactor and then to control the final diameter of the particles. The precipitate obtained was separated by centrifugation at 14500 rpm, then washed twice with deionized water and once with ethanol. Finally, it was dried overnight in an oven at 90°C.

The average particle diameter was finally estimated from SEM image analysis (see **Figure S1** reported in supplementary material). For each synthesis condition, a set of at least 250 particles was considered, and the average value is reported in **Table 1**. The three sets of particles prepared exhibit average diameters close to 400, 1600 and 2400 nm, values that will be used to designate the samples in this paper.

Table 1. Operating conditions in terms of stirring speed and associated Reynolds number (Re_A) used during the hydrothermal synthesis of UO_{2+x} microparticles. Associated diameters as obtained by SEM image analysis are supplied with a ± 1σ confidence interval.

Stirring speed (rpm)	900	950	1050
Re_A (dimensionless)	11370	12000	13260
Particles diameter (nm)	2450 ± 220	1670 ± 80	410 ± 50

In order to fix the O/M ratio in the uranium oxide microparticles, a final heat treatment was performed at 700°C for 1 hour, under either Ar-H_2 4% or air atmosphere. Reducing conditions (Ar-H_2 4%, $P(O_2) = 10^{-29}$ atm) were used to recover UO_{2+x} samples , with x typically ≤ 0.05. The latter value was estimated from previous work conducted in similar conditions, based on both XRD measurements and thermodynamic calculations [22]. Under air,

uranium(IV) was oxidized, resulting in the formation of U_3O_8. Examples of the XRD patterns obtained from these calcined samples are reported as supplementary material (average diameter of 1600 nm - **Figure S2**). These heat treatments were also accompanied by a small shrinkage of the particles, resulting in a 5-10% decrease in diameter [10].

Finally, specific surface area measurements (S_{Sa}, expressed in $m^2.g^{-1}$) were carried out on the different types of particles prepared, in order to normalize dissolution rates by the reactive surface area of the solid/solution interface (see section 2.2. below). Specific surface area values were measured by gas adsorption at 77K using a Micromeritics ASAP 2020 instrument. Here, Kr was preferred to N_2 because of the small areas to be measured (typically less than 1 m^2), both due to the specific surface area itself and the limited amount of material available. Prior to measurement, the samples were outgassed under vacuum at 90°C for 14h. As expected, the S_{Sa} values of the raw samples obtained directly after synthesis decrease with the average particle diameter from 8 to 1 $m^2.g^{-1}$ (**Figure 1**).

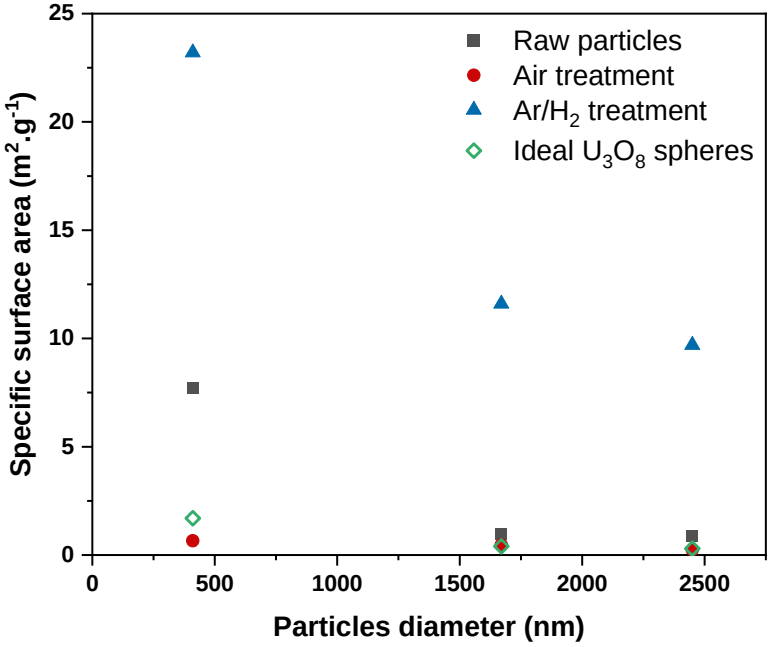

Figure 1. Variation of the specific surface area versus the particles diameter for raw samples obtained after hydrothermal synthesis (black squares), and particles obtained after heat treatment in Ar/H_2 (blue triangles) and air (red circles) atmospheres. Green diamonds accounts for the calculated S_{SA} value for ideal dense U_3O_8 spheres.

Surprisingly, these values evolved very differently after heating, depending on the atmosphere considered. After firing in air, the specific surface area values were found to decrease, in good agreement with the elimination of volatile matter (such as residual organics and water). Moreover, they were close to that calculated from ideal U_3O_8 spheres, indicating that the particles maintained a diameter close to that reported in **Table 1**, and are nearly fully densified. Conversely, a calcination under Ar/H_2, which helped to stabilize U(IV), and to yield UO_{2+x} particles, led to a strong increase of the specific surface area, with S_{SA} values

ranging from 23 to 10 $m^2.g^{-1}$. Such a behavior was probably due to the formation of mesoporosity during the elimination of organic matter. This process has been well documented in the case of the thermal decomposition of actinide oxalate [23], and probably occurred in a similar way during the decomposition of residual aspartate moieties during this study.

2.2. Alteration tests

The leaching experiments were undertaken by placing about around 50 mg of microparticles with different chemical forms (UO_{2+x} or U_3O_8) and sizes (400, 1600 or 2400 nm in diameter) in a 50 mL Savillex brand PFA (Perfluoroalkoxy) vial containing 20 mL of leaching solution (10^{-2} mol.L^{-1} HNO_3, deionized water, or ethanol (H_2O ~ 4%)). These tests were carried out in static mode, i.e. without a continuous renewal of the solution during the experiment. The latter lasted from 55 days for particles leached with HNO_3 to 375 days for those leached in deionized water and absolute ethanol. For each experiment, the leachate was sampled periodically. For uranium oxide particles altered in HNO_3 and water, dissolution was monitored by sampling 0.5 mL of leaching solution. The sample was then acidified by adding 4.5 mL of 0.4 mol.L^{-1} HNO_3, and eventually diluted in nitric acid. When working in ethanol, 0.5 mL of solution was sampled, then evaporated. The solid residue was recovered in 0.4 mol.L^{-1} HNO_3 for further analysis. It is important to note that after each sampling, 0.5 mL of fresh solution was added in the vial to maintain a constant surface to volume ratio (S/V).

Uranium concentration was measured in the leachates using a Thermo Scientific ICAP 7000 inductively coupled optical emission spectrometer (ICP-OES), with a detection limit close to 0.1 ppm. The apparatus was calibrated using standard solutions (0.5, 1, 2.5, 5, 7.5, 10 and 15 ppm) prepared by dilution of certified standard solution of 1000 $mg_U.L^{-1}$ (Plasma-CAL, SCP Science) in 0.2 mol.L^{-1} HNO_3. Uranium concentration was determined by considering wavelengths at 367.007, 385.958 and 409.014 nm. The release of uranium in solution was then expressed as a ratio of the initial uranium mass (equation 1) such as:

$$\%(U)_{dissolved} = \frac{(C_U \times V_{sol})}{m_U(i)} \times 100 \qquad (1.)$$

where C_U represents the uranium concentration measured in g.L^{-1}, V_{sol} corresponds to the total volume of leachate in L and $m_U(i)$ is the initial mass of uranium in the sample (g).

The normalized weight loss ($N_L(U,t)$, expressed in g.m^{-2}) was also determined, this latter being widely used to describe the dissolution of materials [24]:

$$N_L(U,t) = \frac{m_U(t)}{f_U \times S} \qquad (2.)$$

with $m_U(t)$ the mass of uranium released in solution (g) at a given time t, f_U the mass fraction of uranium in the solid phase (g.g^{-1}) and S the area of the solid/liquid interface (m^2). The latter was obtained by multiplying the specific surface area by the total mass of solid involved during the experiment.

The normalized dissolution rate $R_L(U)$, expressed in g.m^{-2}.day^{-1}, was then obtained from the slope when drawing the evolution of N_L over time [24], i.e.:

$$R_L(U,t) = \frac{dN_L(U,t)}{dt} \qquad (3.)$$

2.3. Characterization of raw and altered particles

After leaching, the altered particles were characterized from structural, morphological and isotopic point of views, using XRD, SEM and LG-SIMS measurements, respectively. Prior to these analyses, the solid phases were separated from the leachates by centrifugation, then rinsed several times with deionized water, and let to dry at room temperature.

For X-Ray Diffraction (XRD), a mass of about 5 mg of powder was dispersed in 1 mL of ethanol and deposited on low-background silicon sample holder. XRD data were obtained using a Bruker D8 diffractometer equipped with a Lynx-eye detector adopting the reflection geometry and CuK$\alpha_{1,2}$ radiation (λ = 1.54184 Å). Patterns were recorded at room temperature in the range $5° \leq 2\theta \leq 100°$ with a step size of $\Delta(2\theta) = 0.01$ ° and a total counting time of about 3 hours per sample.

Raman spectra of the altered particles were recorded using a Renishaw Invia apparatus. Drops of the suspensions containing the particles were deposited on stainless steel discs, then the particles were spotted by the means of an optical microscope. A 514 nm wavelength laser with a maximal power of 50 mW was used, resulting in a spot size of about 1 µm. It was then possible to analyse the particles individually. Spectra were recorded between 200 and 1200 cm^{-1} through the average of 10 measurements of 30 s each, with an incident power of approx. 0.5mW.

Before microscopic observation, solid residues were dispersed in ethanol and deposited on a mirror-grade polished aluminum plate. Scanning Electron Microscope (SEM) images were then recorded without any further preparation with a FEI Quanta 200 scanning electron microscope, equipped with an Everhart-Thornley Detector (ETD) and a Back-Scattered Electron Detector (BSED). Images were recorded with an acceleration voltage of 2 kV under high vacuum conditions.

A FIB (Focused Ion Beam) device, available on a Thermo-Scientific "Quanta 3D FEG" SEM, was used to examine the internal porosity of the particles. FIB systems use a finely focused beam of ions (here gallium) that can be operated at low beam currents for imaging or at high beam currents for site specific sputtering or milling. The gallium ($Ga^{+)}$ primary ion beam hits the sample surface and sputters out a small amount of material. Objects under examination can thus be cut into slices only a few nm thick. In this study, the intensity of the gallium ion beam used for particle machining ranged from 1 to 10 nA at an angle of 10°, while the acceleration voltage used for SEM imaging ranged from 15 and 30 kV.

Finally, LG-SIMS analyses were performed to accurately determine the isotopic composition of the raw and altered particles. 20 microparticles from each batch were characterized to compare the accuracy and repeatability of the measurements before and after alteration. The LG-SIMS measurements were performed on a CAMECA IMS 1300HR[3] equipped with a Hyperion II RF plasma oxygen source from Oregon Physics (Beaverton, OR, USA). Such a primary oxygen ion beam is typically used to enhance the production of electropositive ions such as U^+. All analyses were performed with a primary high voltage of +15 kV, a sample high voltage of +8 kV, a mass resolution power of about 4000 and a focused O_2^+ primary beam intensity of 70 pA, with no raster. The ionic species $^{234}U^+$, $^{235}U^+$,

$^{236}U^+$, $^{238}U^+$ and $^{238}UH^+$ were recorded simultaneously in a multi-collection mode using electron multipliers.$^{238}UH^+$ was measured to determine the hydride rate and to correct for the contribution of $^{235}UH^+$ signal to the $^{236}U^+$ signal.

3. Results

3.1. Alteration tests performed in 10^{-2} mol.L^{-1} HNO_3

As a first step, the various batches of particles prepared were subjected to alteration tests in 10^{-2} mol.L^{-1} HNO_3. **Figure 2** shows the evolution of the fraction of solid dissolved, and normalized weight losses, $N_L(U)$, determined from the concentration of uranium in solution. The evolution of the latter is presented as supporting information, **Figure S3**. The curves obtained systematically show a higher release of uranium into solution during the first hours of contact between solid and solution, followed by a slowing down of the dissolution rate. This behavior has already been described several times in the literature [24-27], and corresponds to a washing stage of the sample, during which oxidized solid phases or those with defects are preferentially eliminated. The actual dissolution rate of the material studied is then obtained by analyzing the second part of the curve. For the two chemical forms considered (UO_{2+x} and U_3O_8), the average particle diameter appears to have little influence on the amount of material released in solution, with all curves virtually superimposed in each case. This is confirmed by the normalized leaching rates (**Table 2**), which increase by about a factor 2 for both U_3O_8 and UO_{2+x} particles as the particle diameter increases from 400 to 2400 nm. Such a deviation is usually not considered sufficient to unambiguously distinguish N_L values, especially due to the uncertainties associated with reactive surface measurements. On the other hand, the atmosphere chosen for the heat treatment of the particles induces a significant difference in their chemical durability. Indeed, after treatment in air and conversion into U_3O_8, the quantity of uranium released into solution corresponds to less than 1% mass loss after more than 1200 hours of contact between the solid and the solution (i.e. some fifty days). Conversely, particles in the UO_{2+x} form (calcined under Ar/H_2) show a reduced chemical durability, leading to a loss of about 12% of the initial mass after 1200 hours. This difference is also illustrated by the long-term weight loss trend, since a slowdown is observed in the case of UO_{2+x} after 1200 hours of leaching, linked with the gradual exhaustion of the solid surface, which is not the case for U_3O_8 particles. However, the determination of the normalized mass losses, taking into account the reactive surface of both types of particles, allows us to mitigate these results (**Figure 2b** and **2d**, **Table 2**). Indeed, the values obtained are systematically of the same order of magnitude,typically ranging from 3×10^{-4} to 1×10^{-3} g.m^{-2}.day^{-1}. They are thus typically in the same order of magnitude as those determined by Cordara *et al.* [28] or Barral *et al.* [29] for bulk materials (UO_{2+x} sintered pellets). The small size of the microspheres and their nanostructured nature then do not lead to any specific behavior with respect to their normalized leaching rate.

Table 2. Normalized leaching rates $R_L(U)$ determined during the dissolution of the uranium oxide particles in 10^{-2} mol.L^{-1} HNO_3.

Particle size (nm)	R_L U_3O_8 (g.m^{-2}.day^{-1})	R_L UO_{2+x} (g.m^{-2}.day^{-1})
400	$(5.0 \pm 0.2) \times 10^{-4}$	$(3.4 \pm 0.2) \times 10^{-4}$
1600	$(7.0 \pm 0.2) \times 10^{-4}$	$(5.8 \pm 0.2) \times 10^{-4}$
2400	$(1.2 \pm 0.2) \times 10^{-3}$	$(6.5 \pm 0.2) \times 10^{-4}$

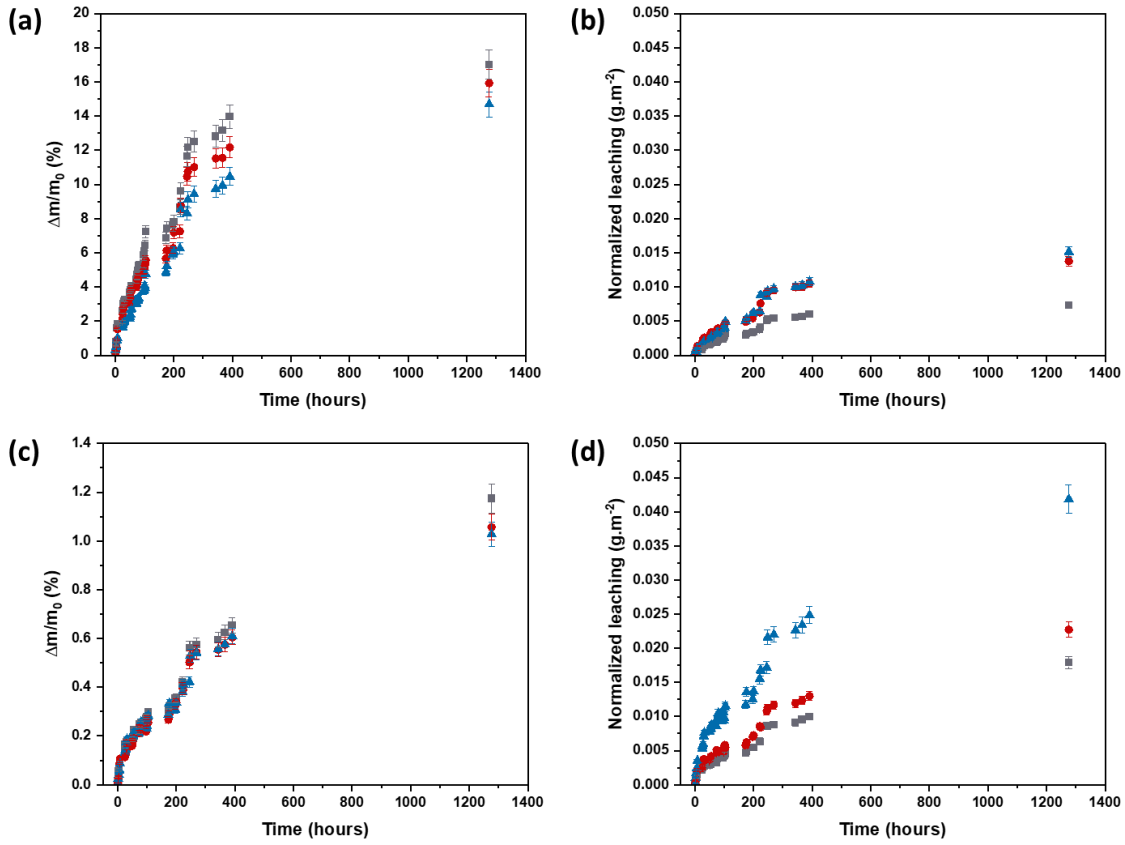

Figure 2. Evolution of the relative mass dissolved $\Delta m/m_0$ (a,c, in %) and of the normalized leaching (b,d, in $g.m^{-2}$) during the dissolution of UO_{2+x} (a,b) and U_3O_8 (c,d) particles in 10^{-2} $mol.L^{-1}$ HNO_3, with average diameters of 400 nm (grey squares), 1600 nm (red circles) and 2400 nm (blue triangles).

Following the dissolution tests carried out on the 1600 nm diameter particles, the residual solid phases were analyzed by XRD and SEM (**Figure 3**). The XRD data showed that for both types of samples studied, no change in the nature of the oxide occurred during the alteration. In fact, the patterns still correspond to the orthorhombic lattice of U_3O_8, and to the fluorite-type structure of UO_{2+x}. For the latter, however, an increase in the O/U ratio cannot be ruled out, but cannot be demonstrated due to the low quality of the data, which stems both from the small amount of material involved and the nanometric nature of the crystallites.

SEM observations show a very different morphological evolution depending on the chemical form of the particles used for the leaching test. In the case of UO_{2+x}, the residue takes the form of nanometric crystallites aggregated in agglomerates of several microns in size. No trace of the initial spherical morphology remains. It is therefore likely that the dissolution process first involved the crystallite boundaries that held the initial microspheres together. Conversely, in the case of U_3O_8, the sample is still clearly composed of distinct microparticles. However, these appear to be highly facetted and have also lost their spherical habit. Furthermore, these particles appear to be dense, in good agreement with the specific surface area measurements made on the initial powders. These observations thus confirm the kinetic data presented earlier, which show a much higher alteration of the UO_{2+x} particles.

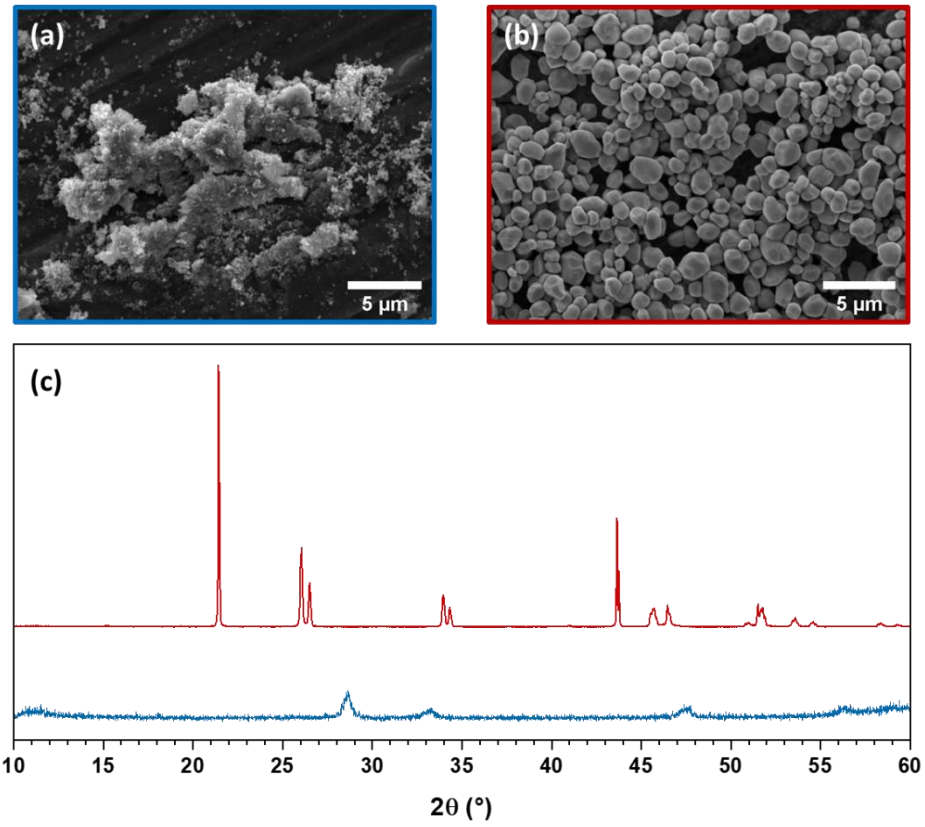

Figure 3. SEM observations of the 1600 nm diameter particles altered in 10^{-2} mol.L^{-1} HNO_3 for 1300 hours : UO_{2+x} (a) and U_3O_8 (b). XRD patterns of the solid residues for UO_{2+x} (blue) and U_3O_8 (red) (c).

3.2. Alteration tests performed in deionized water

In a second step, the chemical durability of UO_{2+x} and U_3O_8 particles was studied in water to mimic their storage in wet conditions. To this end, the particles described above were placed in contact with aerated deionized water (pH ~ 6, after contact with the particles) for several months. The evolution of the uranium concentration in the leachate was monitored regularly as described in 2.2 (**Figure 4**). Similar to the oxide particles altered in nitric acid, the percentage of dissolved uranium $\Delta m/m_0$ appears to be weakly correlated with initial particle diameter. For both UO_{2+x} and U_3O_8 particles, an erratic variation in uranium concentration around a mean value can be observed. This most likely reflects the rapid establishment of an equilibrium in solution, corresponding to the precipitation of a neoformed phase. In good agreement with this hypothesis, the equilibrium concentration does not vary significantly for the 5 samples studied, ranging from 4.9×10^{-4} to 6.3×10^{-4} mol.L^{-1}.

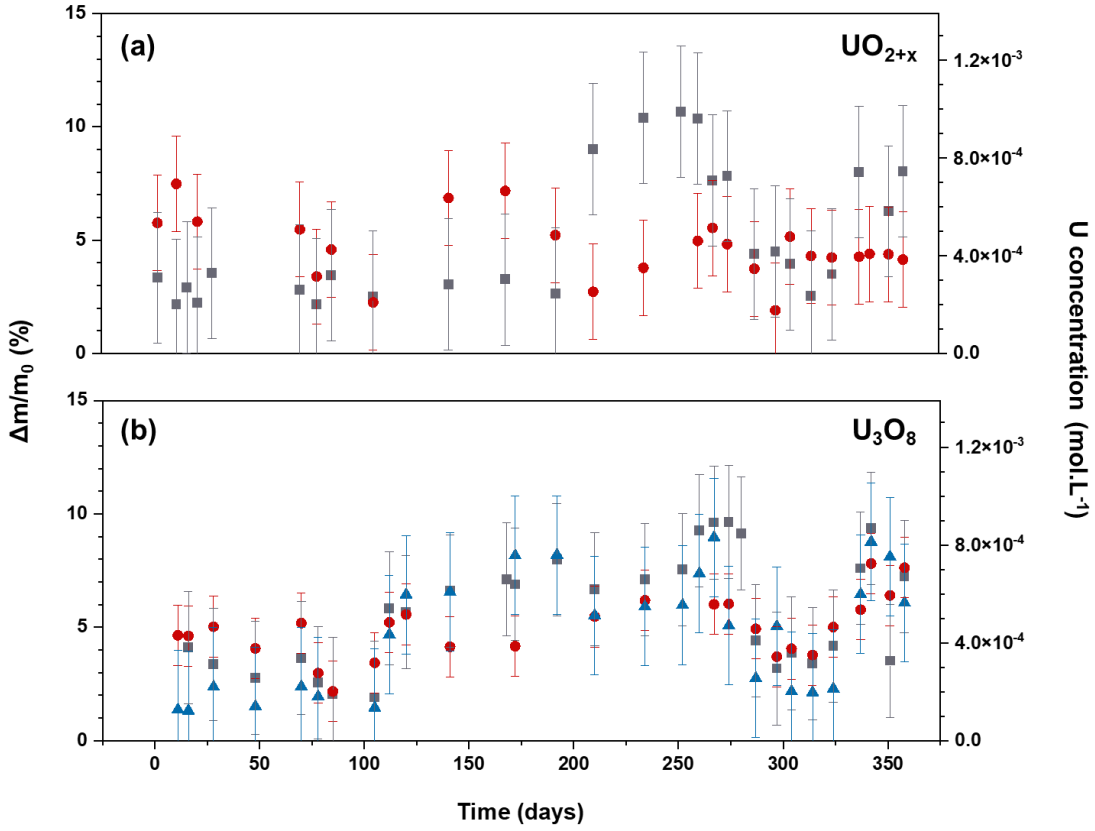

Figure 4. Evolution of the mass dissolved (in %) and the uranium concentration in the leachate (in mol.L^{-1}) during the alteration of UO_{2+x} (a) and U_3O_8 (b) particles in H_2O, with average diameters of 400 nm (grey squares), 1600 nm (red circles) and 2400 nm (blue triangles). Concentrations are supplied with an expanded uncertainty with k = 2.

The characterization of the residual solid phases collected after almost a year of immersion in water confirms the hypothesis of secondary phase formation (**Figure 5**). In fact, SEM images show a complete modification of the initial morphology, both in the case of UO_{2+x} or U_3O_8,. In the case of UO_{2+x}, rectangular platelets up to 20 µm in length are formed. In the case of U_3O_8 microparticles, a morphological evolution towards platelets formation is also noted, but with much smaller grains, less than one micrometer in size. A difference can also be seen in the XRD patterns of these two samples. For the precipitate that replaced the initial UO_{2+x} particles, several phases can be indexed. The most intense XRD peak corresponds to schoepite, $[(UO_2)_8O_2(OH)_{12}](H_2O)_{12}$ (also often written as $UO_3{\cdot}2.25H_2O$) [30], while some other reflections can be attributed to poorly crystallized UO_3 [31]. Several other peaks, including the one with the second highest intensity close to 15°, might be associated to studtite $UO_2(O_2){\cdot}4H_2O$ [32] or to is dehydrated counterpart, meta-studtite [33]. While no peroxide ions were introduced into our reaction medium, modeling results suggest that the introduction of interstitial H_2O molecules into the lattice of uranium oxides could lead to water dissociation and the formation of uranyl peroxide [34]. Indeed, the latter has already been observed by Hammerich *et al.* during the aging of U_3O_8 microparticles in water vapor saturated atmosphere [14] and by Pointurier *et al.* when UF_4 was exposed to environmental

conditions [35]. In our study, the existence of peroxo groups in the solid phase is also suggested by additional Raman experiments (**Figure S4**), which show a small band close to 900 cm^{-1}, that might correspond to the ν(O-O) stretching vibration which is usually reported at around 870 cm^{-1} for reference studtite samples [36]. The most likely hypothesis is therefore that the precipitate formed is a mixture of studtite, together with several schoepite-related phases , whose structure varies only as a function of the hydration rate of the compound. Such a variety of phases has recently been pointed out by Wilkerson *et al.* [34] in their study of UO_3 hydration. With the same idea, Finch and Hawthorne suggest the existence of a wide range of 'dehydrated schoepite' compositions, and propose a general formulation of $(UO_2)O_{0.25-x}(OH)_{1.5+2x}$ for these phases [37].

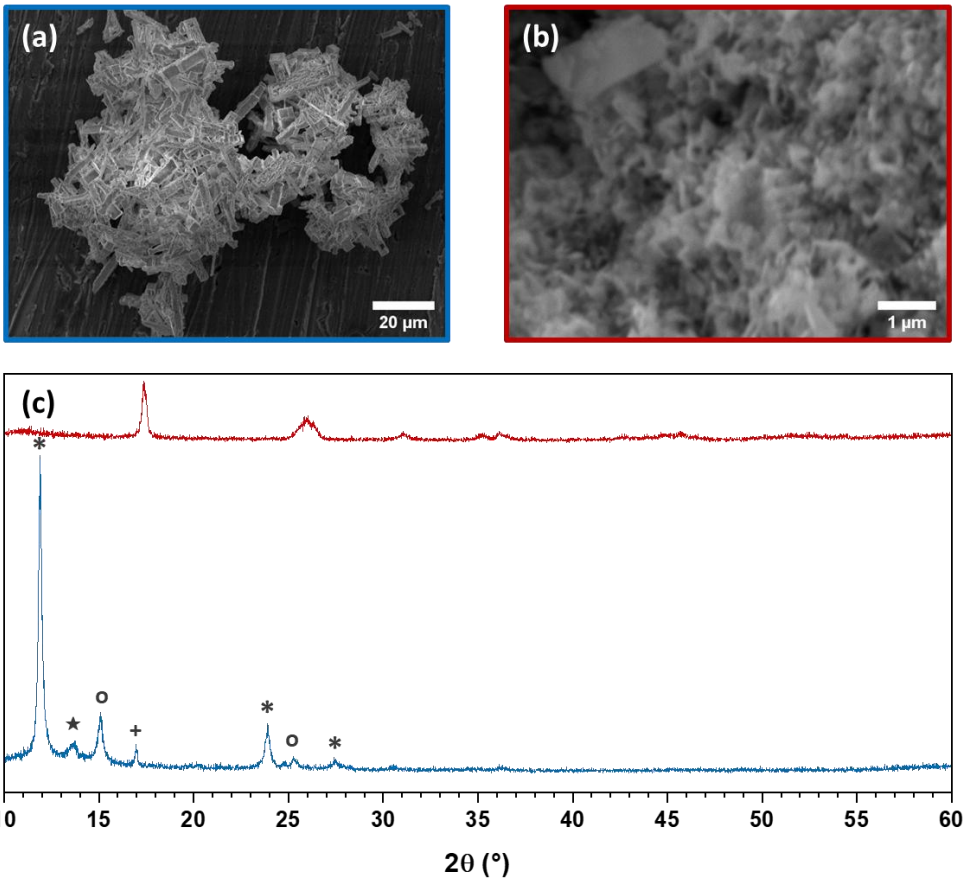

Figure 5. SEM observations of the 400 nm diameter particles altered in H_2O for 358 days: UO_{2+x} (a) and U_3O_8 (b). XRD patterns of the solid residues for UO_{2+x} (blue) and U_3O_8 (red) (c). Indexation of the XRD lines : * = schoepite (ICDD-PDF file #00-050-1601, [38]); o = studtite (#00-016-0206, [39]); + = meta-studtite (#01-081-9033, [33]); ★ = UO_3 (#00-031-1421, [31]).

In the case of U_3O_8 particles, the XRD peaks correspond to the α-form of uranyl hydroxide $(UO_2)(OH)_2$, also reported in the literature under the formula $UO_3 \cdot 0.8H_2O$ [40]. Once again, this writing is associated with the dehydrated schoepite formulation, and thus reflects a two-dimensional structure approximating that of schoepite and meta-schoepite [37]. These observations show that the alteration of uranium oxide microparticles in all cases results in schoepite and possibly studtite type phases, the nature of which depends on the nature of the

initial oxide phase, its reactivity towards the solution and the length of time spent in solution. It is therefore very difficult to predict the exact nature of the neoformed phase, but it is certain that the initial morphology will be profoundly modified in all cases.

3.3. Alteration tests performed in ethanol

As with the previously studied media, the concentration of uranium dissolved in solution (and therefore the percentage of particles dissolved) was monitored for more than 350 days during the storage of UO_{2+x} and U_3O_8 particles as suspensions in ethanol to determine the associated relative weight losses and normalized leaching (**Figure 6**). Concentration are plotted in Supporting information, **Figure S5**. During the first 50-100 days of weathering, dissolved uranium concentrations were generally below the detection limit of the ICP-OES apparatus used for the measurements (10^{-6} M). Beyond this period, alteration begins to be quantifiable but remains low, as after about a year of alteration, the amount of dissolved material reaches about 4% in the worst case (UO_{2+x} particles) and 2% for U_3O_8 particles.

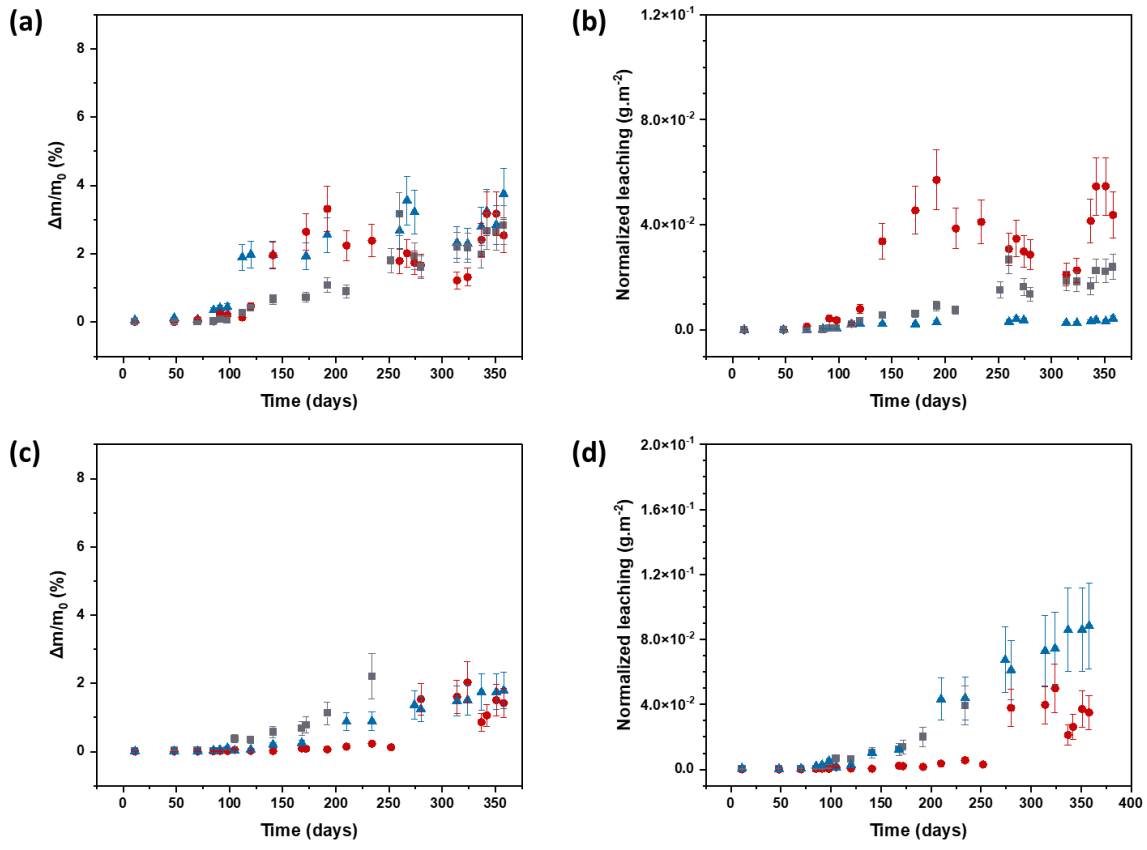

Figure 6. Evolution of the relative mass dissolved (a,c, in %) and the normalized leaching (b,d, in $g.m^{-2}$) during the alteration of UO_{2+x} (a,b) and U_3O_8 (c,d) particles in ethanol, with average diameters of 400 nm (grey squares), 1600 nm (red circles) and 2400 nm (blue triangles).

These values appear to be slightly higher than those reported by Middendorp *et al.* [41] or more recently by Potts *et al.* [12] for U_3O_8 particles prepared by aerosol pyrolysis and then weathered in ethanol. In this case, the relative dissolved mass of U_3O_8 particles reached 0.21% after 228 days, which appears to be 5 to 10 times lower than U_3O_8 particles of similar size (*i.e.* 1600 and 2400 nm) prepared in this work and weathered for 250 days. This difference could be explained by the purity of the solvent used, in particular the water content , which was higher in this study (H_2O ~ 4%) than in that of Potts *et al.* (extra dry absolute ethanol, H_2O < 0.1%). These authors also performed their study in deaerated conditions, while ours was performed in contact with air. These differences in operating conditions probably are likely to have a significant impact on the uranium oxidation rate and then on the chemical durability of the particles in light of the result presented in the previous section. This point will be discussed in more detail below. Despite this deviation from previous results, the microparticles still exhibit a low level of alteration whatever their size. Therefore, similar to the other media studied, it is difficult to correlate the diameter of the prepared oxide particles with their normalized leaching rate. Thus, the normalized weight loss measured in ethanol is generally between 5×10^{-5} and 10^{-4} $g.m^{-2}.day^{-1}$, i.e. about 5 to 10 times lower than those obtained in 10^{-2} $mol.L^{-1}$ HNO_3.

Since the results of the kinetic study show a very low leaching of the uranium oxide samples, whatever their chemical form, the characterization of altered microparticles was focused on the UO_{2+x} chemical form, since they showed the highest relative mass dissolved, particularly due to their higher specific surface area. Thus, this specific study should enable us to highlight any morphological and chemical modifications induced by their stay in ethanol. SEM images of the raw particles and those altered during 8 months in ethanol initially showed no difference. To go further, additional data were obtained using a slice and view technique with a Focused Ion Beam (FIB) setup (**Figure 7**), which allows particles to be cut in vertical slices of about ten nm. Whether before or after leaching, the particles studied, which were chosen randomly and considered to be representative owing to the uniform morphology observed on SEM images, have the same general appearance. In particular, no porosity or cracks can be detected on the surface at the SEM scale. This observation must be qualified with respect to the bulk material. Indeed, both particles appear to be globally dense, but show a central crack. The latter probably results either from the initial self-assembly of the elementary crystallites composing the microspheres, or from the sintering processes occurring during the heat treatment of the as-precipitated particles. As such, this observation could appear to be in contradiction with BET analyses showing that UO_{2+x} particles retained a high specific surface area after heat treatment in a reducing atmosphere. However, this specific surface area is probably due to the presence of mesopores, typically less than ten nm in size, which can only be observed by transmission electron microscopy [23]. Even though, this residual porosity does not lead to percolation of the solution into the material through the pore network after leaching, nor to significant bulk alteration. Despite the higher reactivity of the solid/solution interface, the integrity of the particles is then preserved during storage in alcoholic media. XRD analyses (see supplementary material, **Figure S6**) confirmed that altered particles retained the fluorite-type structure typical of UO_{2+x} materials, with characteristic XRD lines at around 2θ = 28°, 33° and 47°. Nevertheless, qualitative comparison with XRD pattern obtained from particles after synthesis and subsequent heat treatment under Ar-H_2 4%, revealed a slight shift of the peaks to higher 2θ values, which is probably due to a slight oxidation of UO_{2+x} particles during storage in ethanol [42]. Small

additional peaks assigned to the formation of meta-studtite were also observed, confirming the partial oxidation of U(IV) under these operating conditions and once again points out the detrimental role of water.

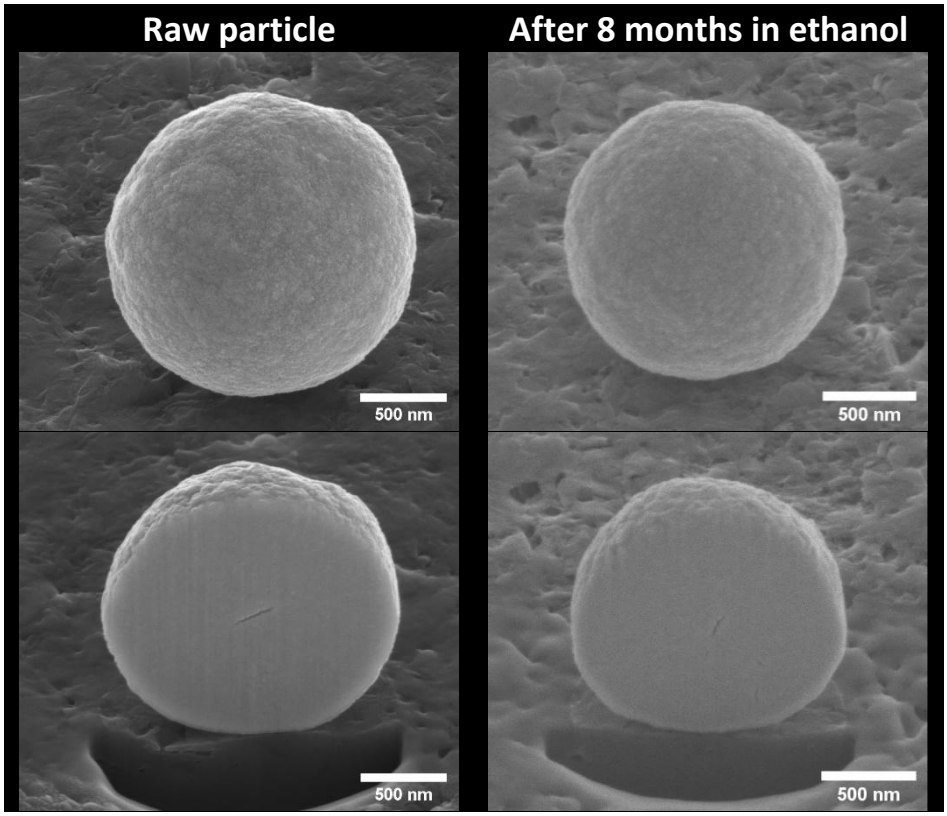

Figure 7. FIB/SEM slice and view of UO_{2+x} particles with average diameters of 1600 nm before and after alteration during 8 months in ethanol.

Finally, isotopic analyses were carried out using LG-SIMS to confirm the possibility to use UO_{2+x} particles as QC materials for nuclear safeguards, even after a long-term storage as a suspension in ethanol. The $^{235}U/^{238}U$ isotopic ratios were then measured in more than 20 different UO_{2+x} particles per batch, *i.e.* with diameters of 400, 1600 and 2400 nm, and before and after 8 months' storage in ethanol (**Figure 8**). Similar data regarding the $^{234}U/^{238}U$ ratio are provided as supplementary material (**Figure S7**). The average values of the initial and post-ethanol isotope ratios are shown in **Table 3**. The results of the isotopic measurements are reproducible for all the particles analyzed, both before and after leaching. No significant variation in the average isotopic ratios was observed before and after 8 months of alteration. Hence, the uranium isotopy remains in line with the values expected for natural uranium present in the Earth's crust ($^{235}U/^{238}U = 7.22 \times 10^{-3}$ to 7.27×10^{-3}) [43-45]. Since the uranium used to synthesize these uranium oxide particles is not an isotopically certified material, it is not possible to calculate a deviation from the certified value. However, it is clear from our data that the stay in ethanol still resulted in a slight increase in the individual uncertainties associated with the isotopy of each particles, especially for the smallest ones. Indeed, the latter varied from 0.5% to 1.3% for the $^{235}U/^{238}U$ ratio after alteration of 400 nm diameter particles, and from 0.5% to 0.8% when the size was increased to 1600 nm. Conversely, the

individual uncertainties remained unchanged and close to 0.6% for the biggest particles (d = 2400 nm). A similar trend was observed for the $^{234}U/^{238}U$ ratio. As such, and even if the mass fraction dissolved during alteration in ethanol did not vary strongly, the predominance of surface versus bulk in the smallest particles led to slightly decrease the performance of the measurements, possibly in relation with the ongoing formation of hydrated secondary phases or isobaric interferences coming from impurities in ethanol. The smallest particles are indeed the more sensitive to these interferences. However, it is important to note that in any case ^{236}U was detected. This isotope, even if present in the environment due to the radioactive fallout from nuclear weapons testing, is expected to be well below the detection limit of the apparatus. However, isobaric artifacts may have occurred due to the presence of ethanol residues on the surface of the particles. These results then show that ethanol can be considered as a good medium for the preservation of UO_{2+x} particles, since both morphology and uranium isotopy were preserved during the 8-month alteration.

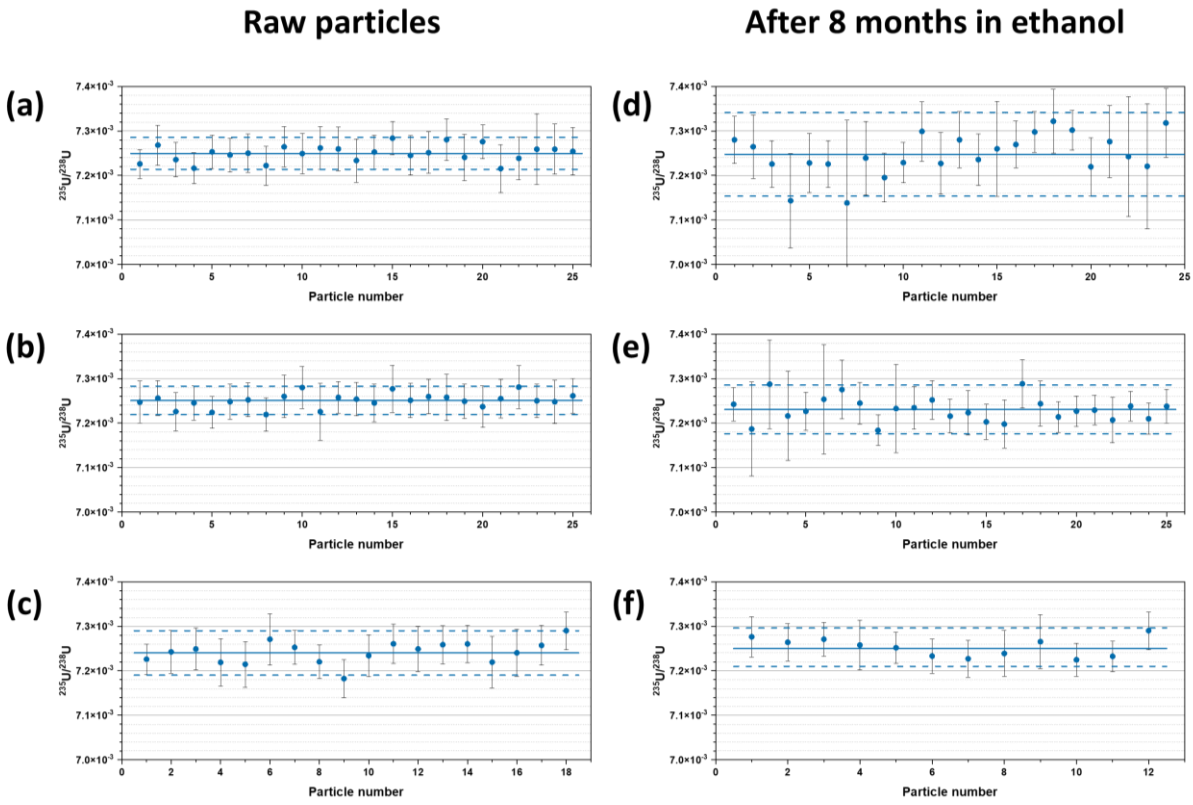

Figure 8. Statistical variation of the $^{235}U/^{238}U$ isotopic ratio measured by LG-SIMS in UO_{2+x} particles (with average diameters of 400 nm (a,d), 1600 nm (b,e) and 2400 nm (c,f)), before (a,b,c) and after (d,e,f) alteration in ethanol during 8 months. The blue solid line corresponds to the mean value of the measured $^{235}U/^{238}U$ isotopic ratio. The blue dotted lines correspond to the confidence interval (at 95%) of the mean value of the measured $^{235}U/^{238}U$ ratio.

Table 3. Average $^{235}U/^{238}U$ isotopic ratios measured in UO_{2+x} particles of different diameters before and after 8 months storage in ethanol. Uncertainty is given with a 95% confidence interval.

Diameter	$^{234}U/^{238}U$		$^{235}U/^{238}U$	
	Raw	Altered	Raw	Altered
2400 nm	$(5.58 \pm 0.34) \times 10^{-5}$	$(5.45 \pm 0.17) \times 10^{-5}$	$(7.244 \pm 0.072) \times 10^{-3}$	$(7.257 \pm 0.056) \times 10^{-3}$
1600 nm	$(5.49 \pm 0.26) \times 10^{-5}$	$(5.40 \pm 0.46) \times 10^{-5}$	$(7.251 \pm 0.031) \times 10^{-3}$	$(7.231 \pm 0.054) \times 10^{-3}$
400 nm	$(5.39 \pm 0.33) \times 10^{-5}$	$(5.56 \pm 0.77) \times 10^{-5}$	$(7.250 \pm 0.039) \times 10^{-3}$	$(7.247 \pm 0.094) \times 10^{-3}$

4. Discussion

The various studies carried out in the course of this work allow us to evaluate the behavior of uranium oxide particles considered in the context of nuclear safeguards when suspended in different media. These results lead to some recommendations for the preservation of the properties required for their potential use as QC reference materials, i.e. controlled morphology and size, which remain homogeneous from particle to particle, and an isotopy that remains invariant over its lifetime.

The first question concerns the chemical form best suited to particle preservation. In the course of this work, UO_{2+x} and U_3O_8 particles showed different chemical durability in terms of absolute mass loss measured in the different media studied. However, these differences do not seem to be an intrinsic chemical characteristic of the particles, but are more certainly a direct consequence of the morphology inherited from synthesis and further heat treatment. Thus, the higher specific surface area generated by calcination in Ar/H_2, combined with the probable existence of mesopores within the particles, appears to be a first-order parameter controlling the chemical durability of the particles, ahead of their chemical nature. Under these conditions, the choice of U_3O_8 particles is guided solely by their specific surface area and must be considered according to the synthesis route envisaged.

After normalization by the reactive surface, the R_L values for UO_{2+x} and U_3O_8 were of the same order of magnitude, although the latter appears systematically higher by a factor of about 2. Beyond their sole application to the retention of reference particles, these measurements allow a direct comparison of the chemical durability of these two uranium oxides under identical physical forms and chemical environments, which has been surprisingly little documented in the literature. In general, the kinetics engine of uranium oxide dissolution in a nitric environment is based on oxidation in the form of uranyl UO_2^{2+} in solution. This oxidation can possibly be auto-catalyzed by the formation of nitrous acid, but this phenomenon is probably not very pronounced in our study due to the low concentration of nitric acid (10^{-2}M HNO_3). The slight difference in behavior observed between UO_{2+x} and U_3O_8 is therefore directly surely due to the solubility of the U^{4+} and U^{5+} species. Indeed, after heat treatment in a reducing atmosphere, UO_{2+x} particles contain mainly uranium(IV) and a small fraction of U(V), in the form of U^{5+}. U_3O_8 particles prepared in air contain 66% U(V) and 33% U(VI). Within the solid, U(VI) is present in the form of U^{6+}, which is highly unstable in solution. The latter will therefore have a very high solubility to adopt the –yle form, i.e. to form the molecular ion UO_2^{2+}. The same trend can be suggested for U(V), which also tends to disproportionate to form U(IV) and U(VI). While these phenomena explain the smaller chemical durability of U_3O_8 in a nitric environment, the difference between the measured dissolution rates remains minimal. It is also important to note that these R_L values are close to those reported in the literature for the leaching of bulk uranium oxides [17, 29]. For example, Cordara *et al.* determined a rate of 6×10^{-4} $g.m^{-2}.day^{-1}$ when dissolving sintered UO_2 pellets in 10^{-1} $mol.L^{-1}$ HNO_3, while expecting little variation in R_L when decreasing the

acidity to pH = 2 [28]. This observation shows that the morphology of the microspheres, which are in fact an agglomerate of nanometric crystallites, does not generate a specific behavior with respect to their chemical durability. As a first approach, the long-term behavior of particles can therefore be assimilated to that of a massive material, and the abundant data existing in the literature for UO_{2+x} and U_3O_8 can be put to good use.

Experiments carried out in deionized water led to the most significant morphological transformations of the altered particles. These were associated with the formation of secondary phases, all resulting from an oxidative dissolution step, followed by hydrolysis of the molecular uranyl ion released into solution. Structural analyses carried out by XRD at the end of the alteration experiments showed that different phases were formed, in particular schoepite, an uranyl oxohydroxide hydrate with the formula $[(UO_2)_8O_2(OH)_{12}](H_2O)_{12}$ (often written as $UO_3 \cdot 2.25H_2O$), nearly amorphous UO_3, and uranyl hydroxide $UO_2(OH)_2$, also referred to in the literature as dehydrated schoepite. Thus, two types of equilibrium can be considered in aqueous media:

$$UO_2^{2+} + 2\ OH^- \leftrightarrows UO_2(OH)_2 \qquad (4.)$$

$$UO_2^{2+} + 3\ H_2O \leftrightarrows UO_3(H_2O)_2 + 2\ H^+ \qquad (5.)$$

With associated solubility constants written as follows:

$$K_{S,1} = [UO_2^{2+}] \times [OH^-]^2 \qquad (6.)$$

$$K_{S,2} = [UO_2^{2+}] \times [H^+]^{-2} \qquad (7.)$$

These constants, which actually differ only in the way they are written and are linked by a $(Ke)^2$ factor, are the two forms reported in the literature for the solubility of uranium(VI) hydroxide or oxohydroxide hydrate [46-48]. In order to confirm the formation of a neoformed phase downstream of the leaching process, the pH and the uranium concentration at the equilibrium (here noted as [U]eq) were measured during the alteration of the different UO_{2+x} and U_3O_8 particles studied. Under the conditions of the study (aerated environment), the UO_2^{2+} concentration was finally calculated using the geochemical speciation model Phreeqc Interactive (version 3.3.3) and the Thermochimie database [49]. It was thus possible to determine the Ks solubility product values for the different experiments carried out, according to the formalisms of equations 6 and 7 (**Table 4**).

Table 4. Values of pH and total uranium concentration at the equilibrium during the alteration of UO_{2+x} and U_3O_8 particles with water. Solubility constant values have been calculated considering either equations 6 (for $K_{s,1}$) or 7 (for $K_{s,2}$) described above.

Sample	pH	[U]eq (mol.L^{-1})	[UO_2^{2+}]eq (mol.L^{-1})	$K_{s,1}$	Log $K_{s,1}$	$K_{s,2}$	Log $K_{s,2}$
UO_2 - 400 nm	5.6	5.3×10^{-4}	3.7×10^{-6}	5.9×10^{-23}	- 22.2(3)	5.9×10^{5}	5.8(3)
UO_2 - 1600 nm	5.5	4.9×10^{-4}	5.3×10^{-6}	5.3×10^{-23}	- 22.3(1)	5.3×10^{5}	5.7(2)
U_3O_8 - 400 nm	5.5	6.3×10^{-4}	5.8×10^{-6}	5.8×10^{-23}	- 22.2(2)	5.8×10^{5}	5.8(2)
U_3O_8 - 1600 nm	5.7	5.2×10^{-4}	2.5×10^{-6}	6.3×10^{-23}	- 22.2(2)	6.3×10^{5}	5.8(1)
U_3O_8 - 2400 nm	5.6	5.4×10^{-4}	3.7×10^{-6}	5.9×10^{-23}	- 22.2(2)	5.9×10^{5}	5.8(2)

Average Log K values :	**-22.2 ± 0.2**	**5.8 ± 0.2**

Despite the differences highlighted by the XRD patterns, the uranium concentration at equilibrium varies only slightly between experiments and also leads to solubility constant values consistent which each other and with those reported in the literature. Thus, the mean value of log $K_{s,1}$ is equal to -22.2 ± 0.2, while that of log $K_{s,2}$ is 5.8 ± 0.2. These results are in very good agreement with literature data, as Langmuir [48] and Fujiwara *et al.* [46] evaluated the solubility product log $K_{s,1}$ = -22, at 298 K, while Gorman-Lewis *et al.* report a variation of log $K_{s,2}$ between 5 and 6.5 [47]. The erratic variation of the uranium concentration around a mean value observed in the experiments conducted in water is therefore due to the formation of secondary phases. In any case, these observations show that contact between the particles and water must be avoided at all costs to ensure their preservation, whether as a suspension in an aqueous medium, or as a powder stored in a humid atmosphere.

The use of an alcoholic solution seems to be a viable option for the storage of particles in suspension. The results obtained during this work in ethanol showed a very low relative mass loss after about 1 year, around a few percent. As mentioned above, this value is higher than that expected from the results reported in the literature, although no changes in morphology or isotopy were observed. The preferred hypothesis to explain this difference is a higher water content in the solvent used in this work and the humid ambient atmosphere. Under these conditions, it seems preferable to keep the particles in an anhydrous solvent. U_3O_8 particles with a diameter of 1600 nm were then placed in extra dry ethanol in a glove box with anoxic (< 0.1 ppm in O_2) and anhydrous (< 1 ppm H_2O) atmosphere. Under these conditions, the mass fraction of altered material reached less than 0.3 wt.% after 500 days, confirming the recommendations proposed above. As the dissolution of uranium oxides is driven by the kinetics of uranium oxidation, lowering the temperature should also help to limit the alteration. These recommendations apply to all types of samples tested in this study, keeping in mind that the reactivity of the samples should be reduced by decreasing the specific surface area of the solids as much as possible.

5. Conclusion

Microparticles of uranium oxides UO_{2+x} and U_3O_8, envisaged as QC reference materials for nuclear safeguards, have been suspended in three different media to study their storage in suspension form. The role of these different media is to simulate different storage conditions (wet storage or storage in a humid atmosphere with water, assumed optimal storage with ethanol) or to evaluate if the synthesized nanostructured particles behave like a bulk material during leaching in a more aggressive medium (10^{-2} mol.L^{-1} HNO_3). The alteration of the uranium oxide particles in nitric acid is already significant after a few hours, but shows no difference with the behavior of sintered pellets in terms of normalized dissolution rate. Thus, $R_L(U)$ values around 5×10^{-4} g.m^{-2}.d^{-1} were obtained for all particle types. However, absolute leaching appears to be more important for UO_{2+x} particles due to their higher specific surface area. Consequently, SEM observations of altered UO_{2+x} particles have shown that the spherical morphology has completely disappeared in favor of dispersed nanocrystallites. The residence time of uranium oxide particles in water is characterized by the rapid precipitation of neoformed phases. The latter were found to vary depending on the

sample studied, but almost all belong to the schoepite family and differ mainly in their water content. In some cases, studtite was also detected. This dissolution/precipitation process was also found to induce a complete change in morphology, with platelets aggregates massively formed in place of the initial microspheres. In contrast to these two media, uranium oxide particles exhibited very slow alteration kinetics in ethanol, the latter again being lower for U_3O_8 particles than for UO_{2+x}. Moreover, SEM/FIB observations confirm the preservation of the spherical morphology after more than 8 months of leaching, as well as the absence of any additional internal porosity formed during the alteration process. Finally, LG-SIMS analyses showed that the residence time in ethanol did not significantly affect the quality of isotopy measurements, despite a slight increase in the uncertainty associated with the data collected from each individual particle.

Globally, these results confirm that ethanol is a suitable medium for preserving particles, especially if it is made free from any trace of water. The results also showed that both U_3O_8 and UO_{2+x} particles have a comparable chemical durability, mostly independent of their size, and that the differences observed in the dissolved fractions are mainly due to the reactivity inherited from their microstructure. Hence, if it is obvious that dry conditions (suspension in dry solvent or conservation as loose powder in H_2O-free glove box) should be preferred to preserve these particles over the long term, the choice of their chemical form should be made depending on the fabrication route retained and on a sound analysis of their microstructure.

Supporting information. Additional experimental data (DOC) including : SEM images of the particles obtained after firing at 700°C under Ar/H_2; XRD patterns of the 1600 nm diameter samples after heating at 700°C; Evolution of the uranium concentration during leaching in 10^{-2}M HNO_3; Raman spectrum of 1600 nm diameter UO_{2+x} microparticles after leaching during 8 months in deionized water; Evolution of the uranium concentration during leaching in ethanol; XRD pattern of 2400 nm diameter UO_{2+x} microparticles after leaching during 8 months in ethanol; Statistical variation of the $^{234}U/^{238}U$ isotopic ratio measured by LG-SIMS in UO_{2+x} particles.

Acknowledgements. The authors would like to thank Marie Tronyo and Maëlys Depernet for their help in the characterization of the leached samples, Olivier Marie for performing SEM/FIB experiments, and Stéphanie Szenknect for Phreeqc calculations. They also thank CEA for its continuous financial support, and for funding Pierre Asplanato PhD work.

References

1. Donohue, D. L., Strengthening IAEA safeguards through environmental sampling and analysis. *J Alloy Compd* **1998,** *271*, 11-18.
2. Kraiem, M.; Richter, S.; Kühn, H.; Stefaniak, E. A.; Kerckhove, G.; Truyens, J.; Aregbe, Y., Investigation of Uranium Isotopic Signatures in Real-Life Particles from a Nuclear Facility by Thermal Ionization Mass Spectrometry. *Anal Chem* **2011,** *83* (8), 3011-3016.

3. Ranebo, Y.; Hedberg, P. M. L.; Whitehouse, M. J.; Ingeneri, K.; Littmann, S., Improved isotopic SIMS measurements of uranium particles for nuclear safeguard purposes. *J. Anal. At. Spectrom.* **2009,** *24* (3), 277-287.
4. Tamborini, G.; Betti, M.; Forcina, V.; Hiernaut, T.; Giovannone, B.; Koch, L., Application of secondary ion mass spectrometry to the identification of single particles of uranium and their isotopic measurement. *Spectrochim Acta B* **1998,** *53* (9), 1289-1302.
5. Lee, C. G.; Iguchi, K.; Inagawa, J.; Suzuki, D.; Esaka, F.; Magara, M.; Sakurai, S.; Watanabe, K.; Usuda, S., Development in fission track-thermal ionization mass spectrometry for particle analysis of safeguards environmental samples. *J Radioanal Nucl Chem* **2007,** *272* (2), 299-302.
6. Baude, S.; Chiappini, R. In *Isotopic measurements on micrometric particles : the French experience to detect fissile material*, Symposium on International Safeguards Verification and Nuclear Material Security, Vienna, IAEA, Ed. Vienna, 2002.
7. Middendorp, R.; Durr, M.; Knott, A.; Pointurier, F.; Sanchez, D. F.; Samson, V.; Grolimund, D., Characterization of the Aerosol-Based Synthesis of Uranium Particles as a Potential Reference Material for Microanalytical Methods. *Anal Chem* **2017,** *89* (8), 4721-4728.
8. Kegler, P.; Pointurier, F.; Rothe, J.; Dardenne, K.; Vitova, T.; Beck, A.; Hammerich, S.; Potts, S.; Faure, A. L.; Klinkenberg, M.; Kreft, F.; Niemeyer, I.; Bosbach, D.; Neumeier, S., Chemical and structural investigations on uranium oxide-based microparticles as reference materials for analytical measurements. *Mrs Adv* **2021,** *6* (4-5), 125-130.
9. Trillaud, V.; Maynadie, J.; Manaud, J.; Hidalgo, J.; Meyer, D.; Podor, R.; Dacheux, N.; Clavier, N., Synthesis of size-controlled UO_2 microspheres from the hydrothermal conversion of U(IV) aspartate. *Crystengcomm* **2018,** *20*, 7749-7760.
10. Asplanato, P.; Zannouh, W.; Fauré, A. L.; Imbert, P. H.; Lautru, J.; Cornaton, M.; Dacheux, N.; Pointurier, F.; Clavier, N., Hydrothermal synthesis of homogenous and size-controlled uranium-thorium oxide micro-particles for nuclear safeguards. *J Nucl Mater* **2023,** *573*, 154142.
11. Pope, T. R.; Arey, B. W.; Zimmer, M. M.; DeVore II, M.; Bronikowski, M. G.; Kuhne, W.; Baldwin, A. T.; Padilla-Cintron, C.; Anheier, N. C.; Warner, M. G.; Wellons, M. S.; Barrett, C. A., Production of particle reference and quality control materials. *ESARDA Bull* **2019,** *59*, 29-38.
12. Potts, S. K.; Kegler, P.; Hammerich, S.; Klinkenberg, M.; Niemeyer, I.; Bosbach, D.; Neumeier, S., Long-term stability of uranium-oxide-based microparticle reference materials: Shelf-life in alcoholic suspension and storage media. *Mrs Adv* **2022,** *7* (7-8), 134-139.
13. Middendorp, R.; Klinkenberg, M.; Durr, M., Uranium oxide microparticle suspensions for the production of reference materials for micro-analytical methods. *J Radioanal Nucl Chem* **2018,** *318* (2), 907-914.
14. Hammerich, S.; Potts, S. K.; Kegler, P.; Neumeier, S.; Schmitt, A. K.; Trieloff, M., Shelf-life of uranium oxide microparticle reference materials and possible implications for the identification of optimal storage conditions. *Mrs Adv* **2023,** *8* (6), 290-295.
15. Heisbourg, G.; Hubert, S.; Dacheux, N.; Purans, J., Kinetic and thermodynamic studies of the dissolution of thoria-urania solid solutions. *J Nucl Mater* **2004,** *335* (1), 5-13.

16. Schlegel, M. L.; Jegou, C., Uraninite alteration by H_2O_2 solutions and formation of secondary phases: An in situ microRaman spectroscopy and synchrotron X-ray diffraction study. *J Nucl Mater* **2022,** *572*.
17. Montaigne, T.; Szenknect, S.; Broudic, V.; Imbert, P. H.; Tocino, F.; Martin, C.; Miserque, F.; Jégou, C.; Dacheux, N., Oxidative dissolution of $(U,Ce)O_2$ materials in aqueous solutions containing H_2O_2. *Npj Materials Degradation* **2023,** *7* (1).
18. Rodríguez-Villagra, N.; Bonales, L. J.; Milena-Pérez, A.; Galán, H., A snapshot review on uranyl secondary phases formation in aqueous systems. *Mrs Adv* **2023,** *8* (6), 207-213.
19. Bertolotto, S.; Szenknect, S.; Lalleman, S.; Magnaldo, A.; Raison, P.; Odorico, M.; Podor, R.; Claparede, L.; Dacheux, N., Effect of surface orientation on dissolution rate and surface dynamics of UO_2 single crystals in nitric acid. *Corros Sci* **2020,** *176*.
20. Perrot, A.; Canizares, A.; Miro, S.; Claparede, L.; Podor, R.; Sauvage, T.; Peuget, S.; Jegou, C.; Dacheux, N., In situ Raman monitoring of studtite formation under alpha radiolysis in ^{18}O-labeled water. *J Nucl Mater* **2024,** *600*.
21. Dacheux, N.; Brandel, V.; Genet, M., Synthesis and Properties of Uranium Chloride Phosphate Tetrahydrate - $UClPO_4.4H_2O$. *New J Chem* **1995,** *19* (10), 1029-1036.
22. Trillaud, V.; Podor, R.; Gosse, S.; Mesbah, A.; Dacheux, N.; Clavier, N., Early stages of UO_{2+x} sintering by in situ high-temperature environmental scanning electron microscopy. *J Eur Ceram Soc* **2020,** *40* (15), 5891-5899.
23. Claparede, L.; Clavier, N.; Dacheux, N.; Mesbah, A.; Martinez, J.; Szenknect, S.; Moisy, P., Multiparametric Dissolution of Thorium-Cerium Dioxide Solid Solutions. *Inorg Chem* **2011,** *50* (22), 11702-11714.
24. Dacheux, N.; Clavier, N.; Ritt, J., Behavior of thorium-uranium(IV) phosphate-diphosphate sintered samples during leaching tests. Part I - Kinetic study. *J Nucl Mater* **2006,** *349* (3), 291-303.
25. Clavier, N.; de Kerdaniel, E. D.; Dacheux, N.; Le Coustumer, P.; Drot, R.; Ravaux, J.; Simoni, E., Behavior of thorium-uranium(IV) phosphate-diphosphate sintered samples during leaching tests. Part II. Saturation processes. *J Nucl Mater* **2006,** *349* (3), 304-316.
26. Dalger, T.; Claparede, L.; Szenknect, S.; Moisy, P.; Dacheux, N., Dissolution of $Th_{0.25}U_{0.75}O_2$ sintered pellets: Impact of nitrate ions and nitrous acid. *Hydrometallurgy* **2021,** *204*.
27. Claparede, L.; Tocino, F.; Szenknect, S.; Mesbah, A.; Clavier, N.; Moisy, P.; Dacheux, N., Dissolution of $Th_{1-x}U_xO_2$: Effects of chemical composition and microstructure. *J Nucl Mater* **2015,** *457*, 304-316.
28. Cordara, T.; Szenknect, S.; Claparede, L.; Podor, R.; Mesbah, A.; Lavalette, C.; Dacheux, N., Kinetics of dissolution of UO_2 in nitric acid solutions: A multiparametric study of the non-catalysed reaction. *J Nucl Mater* **2017,** *496*, 251-264.
29. Barral, T. Etude multiparamétrique de la dissolution d'oxydes mixtes $(U,Ln)O_2$ en milieu nitrique : impact de la composition et de la microstructure. Univ. Montpellier, 2023.
30. Plasil, J., The crystal structure of uranyl-oxide mineral schoepite, $[(UO_2)_4O(OH)_6](H_2O)_6$, revisited. *J Geosci-Czech* **2018,** *63* (1), 65-73.
31. Engmann, R.; Wolff, P. M. D., Crystal Structure of Gamma-UO_3. *Acta Crystallogr* **1963,** *16* (10), 993-&.
32. Burns, P. C.; Hughes, K. A., Studtite, $[(UO_2)(O_2)(H_2O)_2](H_2O)_2$: The first structure of a peroxide mineral. *Am Mineral* **2003,** *88* (7), 1165-1168.

33. Weck, P. F.; Kim, E.; Jové-Colón, C. F.; Sassani, D. C., Structures of uranyl peroxide hydrates: a first-principles study of studtite and metastudtite. *Dalton T* **2012,** *41* (32), 9748-9752.
34. Wilkerson, M. P.; Hernandez, S. C.; Mullen, W. T.; Nelson, A. T.; Pugmire, A. L.; Scott, B. L.; Sooby, E. S.; Tamasi, A. L.; Wagner, G. L.; Walensky, J. R., Hydration of α-UO_3 following storage under controlled conditions of temperature and relative humidity. *Dalton T* **2020,** *49* (30), 10452-10462.
35. Pointurier, F.; Lelong, C.; Marie, O., Study of the chemical changes of µm-sized particles of uranium tetrafluoride (UF_4) in environmental conditions by means of micro-Raman spectrometry. *Vib Spectrosc* **2020,** *110*.
36. Colmenero, F.; Bonales, L. J.; Cobos, J.; Timón, V., Study of the thermal stability of studtite by in situ Raman spectroscopy and DFT calculations. *Spectrochim Acta A* **2017,** *174*, 245-253.
37. Finch, R. J.; Hawthorne, F. C.; Ewing, R. C., Structural relations among schoepite, metaschoepite and "dehydrated schoepite". *Can Mineral* **1998,** *36*, 831-845.
38. Finch, R. J.; Hawthorne, F. C.; Miller, M. L.; Ewing, R. C., Distinguishing among schoepite, $[(UO_2)_8O_2(OH)_{12}](H_2O)_{12}$, and related minerals by X-ray powder diffraction. *Powder Diffr* **1997,** *12* (4), 230-238.
39. Debets, P. C., X-Ray Diffraction Data on Hydrated Uranium Peroxide. *J Inorg Nucl Chem* **1963,** *25* (6), 727-730.
40. Taylor, J. C., Structure of Alpha-Form of Uranyl Hydroxide. *Acta Crystallogr* **1971,** *B27* (Jun15), 1088-1091.
41. Middendorp, R.; Durr, M.; Bosbach, D., The stability of uranium microspheres for future application as reference standard in analytical measurements. *Procedia Chem* **2016,** *21*, 285-292.
42. Elorrieta, J. M.; Bonales, L. J.; Rodriguez-Villagra, N.; Baonza, V. G.; Cobos, J., A detailed Raman and X-Ray study of UO_{2+x} oxides and related structure transitions. *Phys Chem Chem Phys* **2016,** *18* (40), 28209-28216.
43. Brennecka, G. A.; Borg, L. E.; Hutcheon, I. D.; Sharp, M. A.; Anbar, A. D., Natural variations in uranium isotope ratios of uranium ore concentrates: Understanding the $^{235}U/^{238}U$ fractionation mechanism. *Earth Planet Sc Lett* **2010,** *291* (1-4), 228-233.
44. Richter, S.; Alonso, A.; De Bolle, W.; Wellum, R.; Taylor, P. D. P., Isotopic "fingerprints" for natural uranium ore samples. *Int J Mass Spectrom* **1999,** *193* (1), 9-14.
45. Livermore, B. D.; Connelly, J. N.; Moynier, F.; Bizzarro, M., Evaluating the robustness of a consensus $^{238}U/^{235}U$ value for U-Pb geochronology. *Geochim Cosmochim Ac* **2018,** *237*, 171-183.
46. Fujiwara, K.; Yamana, H.; Fujii, T.; Kawamoto, K.; Sasaki, T.; Moriyama, H., Solubility product of hexavalent uranium hydrous oxide. *J Nucl Sci Technol* **2005,** *42* (3), 289-294.
47. Gorman-Lewis, D.; Burns, P. C.; Fein, J. B., Review of uranyl mineral solubility measurements. *J Chem Thermodyn* **2008,** *40* (3), 335-352.
48. Langmuir, D., Uranium Solution-Mineral Equilibria at Low-Temperatures with Applications to Sedimentary Ore-Deposits. *Geochim Cosmochim Ac* **1978,** *42* (6), 547-569.
49. Giffaut, E.; Grivé, M.; Blanc, P.; Vieillard, P.; Colàs, E.; Gailhanou, H.; Gaboreau, S.; Marty, N.; Madé, B.; Duro, L., Andra thermodynamic database for performance assessment: ThermoChimie. *Appl Geochem* **2014,** *49*, 225-236.

For Table of Contents only